Research on Improved Permanent Magnet Linear Synchronous Motor for Direct-Drive Application

Cheng Wen, Jin Liu, Weiming Wang, Junyu Liu, Zhiyan Zhao, and Jingna Liu

Department of Electrical and Electronic Engineering, Shijiazhuang Tiedao University, Shijiazhuang 050043, China

This paper takes a Halbach permanent magnet linear motor (PMLM) without a core as the research subject; based on the traditional structure of a single-layer PM array, an improved PMLM with an optimized double-layer Halbach PM array is proposed to reduce the harmonic components of the air gap magnetic flux density (AGMFD) for direct-drive applications in the feeding system of the machine tool which need high force capability. The 3-D models of PMLMs with single-layer and double-layer Halbach PM arrays are established by using finite element (FE) software; the air gap magnetic field, the back electromotive force (EMF), and the electromagnetic thrust of the two types of motors are analyzed. The simulated results show that the PMLM with an optimized double-layer Halbach PM array can achieve better performances of the motor and reduce the cost of the PMLM. Finally, the experimental results verify that the proposed double-layer Halbach PMLM is effective and practical.

Index Terms— **Air gap magnetic flux density (AGMFD), direct-drive application, Halbach permanent magnet (PM), linear motor.**

I. Introduction

With rapid developments in aviation, aerospace, automobile, and ultra-precision micro-machining, the high-end manufacturing equipment industry is facing huge challenges [1]. At present, the high-end machining technology is developing in two directions of high speed and high precision, so the high performance of a feed drive system is needed to cooperate [2], [3]. In general, the feed drive system can be divided into an electromechanical feed drive that is represented by a ball screw and a directly driven feed drive that is represented by a linear motor. Scholars did some comparative research on the performance, cost, and structure of those two feed drive systems, a directly driven feed drive that is represented by a linear motor has more development prospects than an electromechanical feed drive that is represented by a ball screw in the field of high speed and high precision [4], [5].

In the feed system driven by a linear motor, the direct connection of the linear motor and the load enables the system to have advantages of no friction, good dynamic performance, high repeat running precision, and a wide range of speeds [6], [7]. The speed of the workbench driven by the linear motor can reach 30 times that of the traditional transmission and its acceleration can reach ten times higher than the traditional transmission mode [8]. Therefore, the feed system driven by a linear motor is suitable for precision machining such as high precision, unconventional size, and high cutting speed. It has great potential for development and broad market prospects. The permanent magnet linear motor (PMLM) is attracting the attention of many researchers in the feed system because it has advantages of high efficiency, high power density, high thrust density, and easy control [9].

The study of harmonic components of the air gap magnetic flux density (AGMFD) in the linear motor is helpful to realize high precision direct drive control systems [10]. The Halbach PM array is a new arrangement in the PMLM. It can achieve better sinusoidal characteristics and higher amplitude values of the air-gap magnetic field than the conventional PM. Research on the Halbach PMLM used to be confined to the Halbach PM array with a single-layer structure [11]. The literature [12] proposed a structure of the PMLM that is ironless; for comparative research, one prototype with Halbach arrays and one prototype with radial arrays are made. Theoretical and experimental results show that Halbach arrays can strengthen the AGMFD and improve the sinusoidal distribution of the magnetic field, but the structure and size of Halbach PM arrays need further optimization. The literature [13] proposed a slotless high-speed PM synchronous motor with a novel double-layer Halbach array; analysis shows that the optimized harmonic distortion rate of electric potential is only 0.5%, but there is no analysis for the distribution of the AGMFD. The AGMFD waveform can severely affect the performance of the motor, especially the voltage waveform which is of primary concern for a successful motor. Therefore, the optimization of Halbach PM arrays to reduce the harmonic components of the AGMFD was chosen as the aim of the study in this paper.

An improved PMLM with double-layer Halbach PM arrays is proposed in this paper. This structure not only can improve the sinusoidal characteristic of the AGMFD but also can reduce the quality of PM arrays for direct-drive applications. Finally, the simulated and experimental results are presented to verify the proposed structure.

II. Basic Structure of Halbach PMLM

The structure of a PMLM is mainly divided into the PMLM with cogging and the PMLM that is slotless [14]. Compared with the PMLM with cogging, the PMLM that is slotless removes the iron core, and the non-ferromagnetic material is

Manuscript received January 10, 2019; revised March 19, 2019 and May 6, 2019; accepted June 14, 2019. Date of publication July 2, 2019; date of current version September 18, 2019. Corresponding author: W. Wang (e-mail: wangwm@stdu.edu.cn).

Color versions of one or more of the figures in this article are available online at http://ieeexplore.ieee.org.

Digital Object Identifier 10.1109/TMAG.2019.2923952

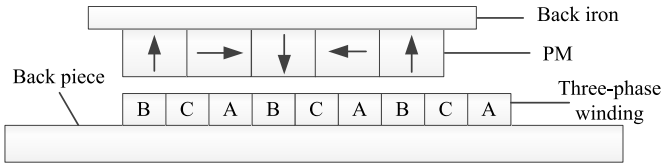

Fig. 1. Basic structure of a coreless Halbach PMLM.

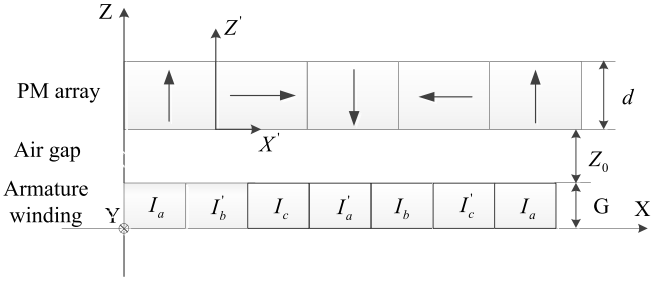

Fig. 2. Mathematical model of a Halbach PMLM.

used to fix and install the winding, so that the quality of the mover becomes light. In addition, there is no cogging effect and weak magnetic saturation. The normal suction is reduced to some extent.

The sinusoidal and magnetic field strength of the air gap magnetic field for the Halbach PMLM is better than that of the conventional PMLM of the same volume. Therefore, a coreless Halbach PMLM is taken as the research object in this paper. Its structure is shown in Fig. 1. The motor consists of a primary and a secondary part; the primary part is a stator that includes three-phase winding and the secondary part is a mover that includes an unconventional Halbach PM array. The Halbach PM array is an approximate ideal structure for engineering. Its goal is to use a minimum number of magnets, but generates the strongest magnetic field. The performance of the motor can be significantly improved by the application of Halbach PM arrays in the PMLM.

III. Electromagnetic Analysis

The mathematical model of the Halbach PMLM is shown in Fig. 2, where the stator coil winding thickness is G, the current of the three-phase winding is I_a, I_b, and I_c, respectively, the direction of the current is $+y$ (perpendicular to the surface), the thickness of the air gap is Z_0, and the thickness of the PM array is d. Each PM has the same width and thickness, and they are 90° different from the magnetic direction of the adjacent PM. Four PMs constitute a magnetic cycle.

According to Maxwell's equations [15]

$$\nabla^2 \vec{A} = \mu_0 \nabla \times \vec{M} \tag{1}$$

where $\vec{A}$ is the magnetic position of the vector, $\vec{B}$ is the magnetic induction, and $\vec{M}$ is the magnetization. The magnetization of the PM array can be expressed by the Fourier series of magnetization in the x-direction and the z-direction

$$\begin{aligned}\vec{M} &= \sum_{n=-\infty}^{n=\infty} [i_x M_{xn} + i_z M_{zn}] \\ &= \sum_{n=-\infty}^{n=\infty} [i_x \vec{M}_{xn} e^{-jk_n z} + i_z \vec{M}_{zn} e^{-jk_n z}]\end{aligned} \tag{2}$$

where $\vec{M}_{xn}$, $\vec{M}_{zn}$ are the nth Fourier series; k_n is the spatial angular frequency of the nth harmonic. $\vec{A}$ and $\vec{B}$ of the PM array can be expressed as follows:

$$\vec{A} = \sum_{n=-\infty}^{\infty} \vec{A}_{yn} e^{-jk_n y} i_y \tag{3}$$

$$\vec{B} = \sum_{n=-\infty}^{\infty} [\vec{B}_{xn} e^{-jk_n x} i_x + \vec{B}_{zn} e^{-jk_n x} i_z]. \tag{4}$$

The Poisson equation can be obtained as

$$\left(\frac{\partial^2}{\partial x^2} + \frac{\partial^2}{\partial z^2}\right) A_{yn} = -jk_n u_0 \vec{M}_{zn} e^{-jk_n x}. \tag{5}$$

The Fourier series of magnetic induction in the x-direction and the z-direction can be obtained by the Laplace transform

$$\vec{B}_{xn} = \left(-\frac{\mu_0}{2}\vec{M}_{xn} - \frac{j\mu_0\gamma_n}{2k_n}\vec{M}_{zn}\right)(1 - e^{-\gamma_n d}) \tag{6}$$

$$\vec{B}_{zn} = \left(-\frac{j\mu_0 k_n}{2\gamma_n}\vec{M}_{xn} + \frac{\mu_0}{2}\vec{M}_{zn}\right)(1 - e^{-\gamma_n d}) \tag{7}$$

where $\gamma_n = |k_n|$. The Fourier series of magnetization in the x-direction and the z-direction can be expressed as follows:

$$\vec{M}_{xn} = \begin{cases} \frac{\sqrt{2}M_0}{\pi |n|}, & n = \pm(8m+1) \text{ or } (8m+3) \\ -\frac{\sqrt{2}M_0}{\pi |n|}, & n = \pm(8m+5) \text{ or } (8m+7) \\ 0, & \text{when } n \text{ is an even number} \end{cases} \tag{8}$$

$$\vec{M}_{zn} = j^n \vec{M}_{xn} \tag{9}$$

where M_0 is the peak of magnetization. The total Fourier series of magnetic induction in the x-direction and the z-direction are obtained by substituting (8) and (9) into (6) and (7)

$$\vec{B}_{xn} = \left(-\frac{\mu_0}{2}\vec{M}_{xn} - \frac{j\mu_0\gamma_n}{2k_n}\vec{M}_{zn}\right)(1 - e^{-\gamma_n d})e^{-k_n z}, \quad z \le 0 \tag{10}$$

$$\vec{B}_{zn} = \left(-\frac{j\mu_0 k_n}{2\gamma_n}\vec{M}_{xn} + \frac{\mu_0}{2}\vec{M}_{zn}\right)(1 - e^{-\gamma_n d})e^{-k_n z}, \quad z \le 0. \tag{11}$$

The harmonic of magnetic field is calculated using (10) and (11); the results show that the magnetic field contains harmonic components such as the fifth harmonic and the ninth harmonic, and the amplitude of the fifth harmonic is large.

IV. Optimizing Halbach PMLM

The air gap magnetic field, the back electromotive force (EMF), and the electromagnetic force are the major concerns for the PMLM. However, the waveform of the air gap magnetic field can seriously affect the performance of the motor, especially the voltage waveform and the electromagnetic force which are of primary concerns for a successful motor. Therefore, the optimization of Halbach PM arrays to reduce the harmonic components of the air gap magnetic field is chosen as the aim of the study in this paper. A double-layer Halbach PM array is proposed for the PMLM based on the study of the traditional PM array in order to improve the sinusoidal distribution of the air gap magnetic field. The 2-D topological structure of the ordinary single-layer Halbach PM

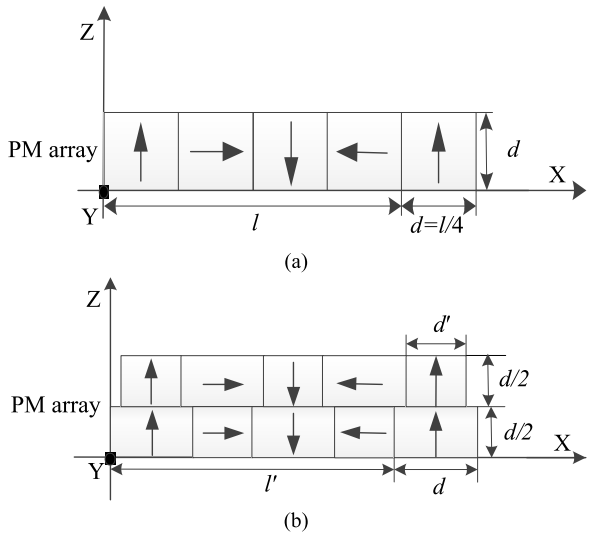

Fig. 3. 2-D topological structure of a PM array. (a) An ordinary single-layer Halbach PM array. (b) Proposed two-layer PM arrays.

array and the proposed double-layer PM arrays in this paper are shown in Fig. 3.

Each pair of the magnetic pole for the single-layer Halbach PM array is composed of four magnets. The width and the thickness of each PM are both given by d, and they are 90° different from the magnetic direction of the adjacent PM. Four PMs constitute a magnetic cycle. The proposed double-layer Halbach PM arrays are composed of two sets of PMs that have different sizes, which are arranged above and below. Assume that the width and thickness of each PM in a single-layer PM array are both $d = 6.6$ mm, while the height of the PM in double-layer PM arrays is 3.3 mm, of which the width of large PMs is 6.6 mm, but the width of small PMs can be freely adjusted for the optimal design, and the ratio of widths for two sets of PMs is marked as $d'/d = n$.

In this paper, the proposed PMLM with double-layer Halbach PM arrays is optimized by a finite element method (FEM). The goal is that the air gap magnetic field with optimal sinusoidal distribution characteristics is obtained by optimized the PM array. The two types of PM arrays in Fig. 3 are established by FE software. The step acceleration method is applied to optimize the design of small-sized PMs in the two-layer Halbach PM array. The width of the small-sized PMs in the double-layer Halbach PM array is optimized from 1.32 to 6.6 mm, in steps of 0.66 mm. That is, n is 0.2, 0.3, 0.4, 0.5, 0.6, 0.7, 0.8, 0.9, and 1 (single-layer).

The distribution of the magnetic field for single-layer and double-layer PM arrays is analyzed by FEM. When the 2-D FEM is established, the following assumptions are made.

1) It is considered that the transverse magnetic field distribution along the motor is uniform, that is, the magnetic field does not change in the Y-direction.
2) The effect of leakage flux at the end of the motor is ignored.
3) The hysteresis effect and the eddy current in back iron are ignored.

The distribution of the air gap magnetic field for single-layer and double-layer PM arrays is simulated by FE separately, as shown in Fig. 4.

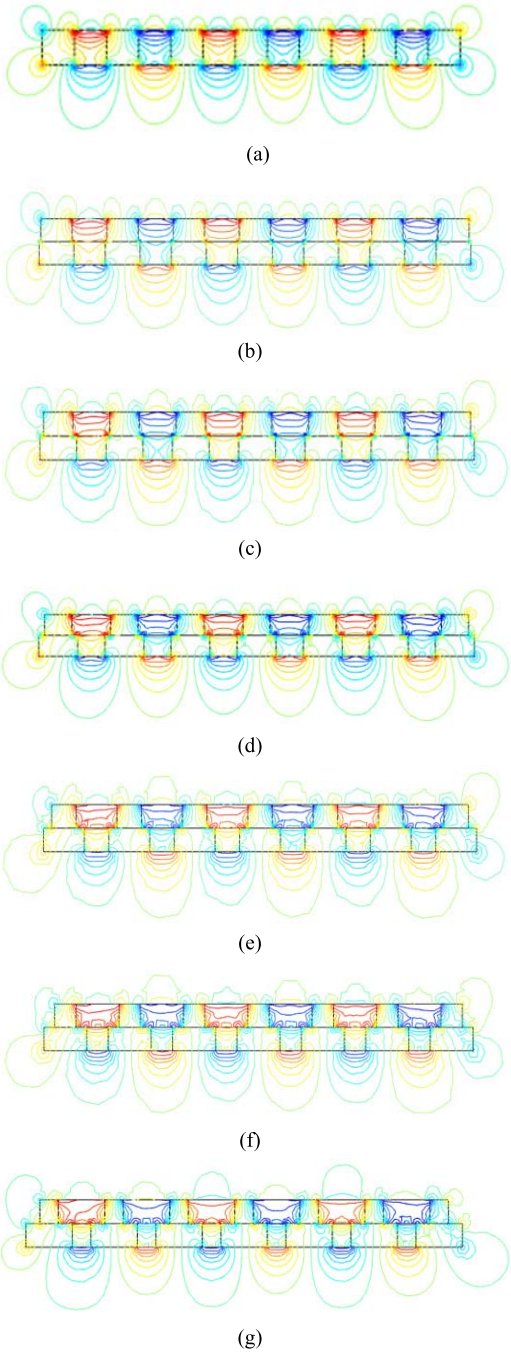

Fig. 4. Distribution of the magnetic field for PM arrays. (a) Distribution of the magnetic field for the single-layer Halbach PM array. (b)–(g) Distribution of the magnetic field for the double-layer PM arrays with different n. (a) $n = 1$. (b) $n = 0.9$. (c) $n = 0.8$. (d) $n = 0.7$. (e) $n = 0.6$. (f) $n = 0.5$. (g) $n = 0.4$.

It can be seen that both the single-layer PM array and the double-layer PM arrays have an obvious single-sided sinusoidal distribution, the magnetic distribution on the magnet is very small, but the magnetic field strength under the magnet is significantly higher, and the sinusoidal distribution is better. The magnetic field at both ends of the array is severely distorted, that is, there is an end effect of the magnetic field. However, the end effect of the magnetic field is ignored in the assumptions.

The sinusoidal characteristics and the strength of the air gap magnetic field directly affect the operational stability and

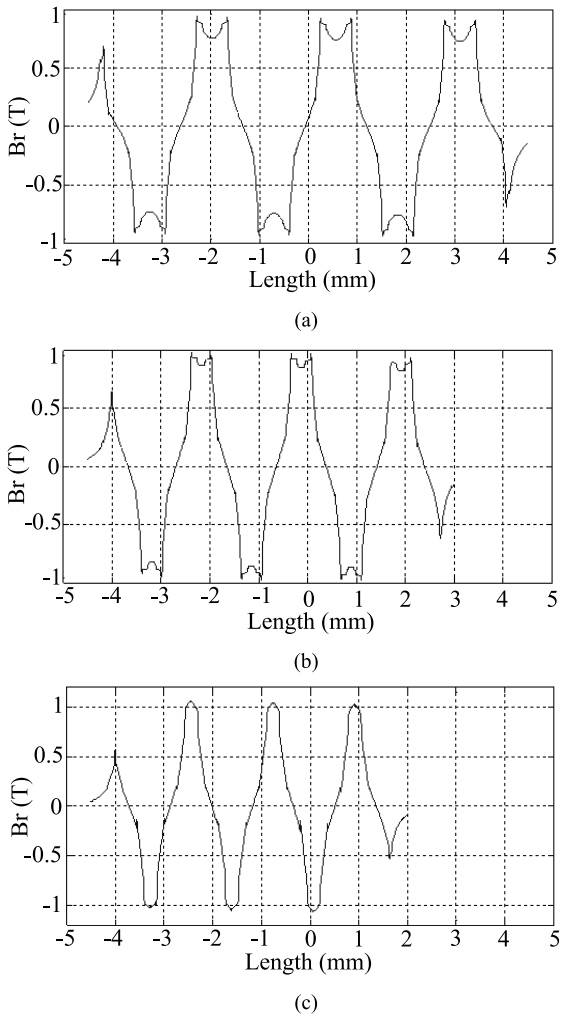

Fig. 5. Waveform of the air gap flux density. (a) Waveform of the air gap flux density for the single-layer Halbach PM array ($n = 1$). (b) and (c) Waveform of the air gap flux density for the double-layer PM arrays with different n. (a) $n = 1$. (b) $n = 0.7$. (c) $n = 0.4$.

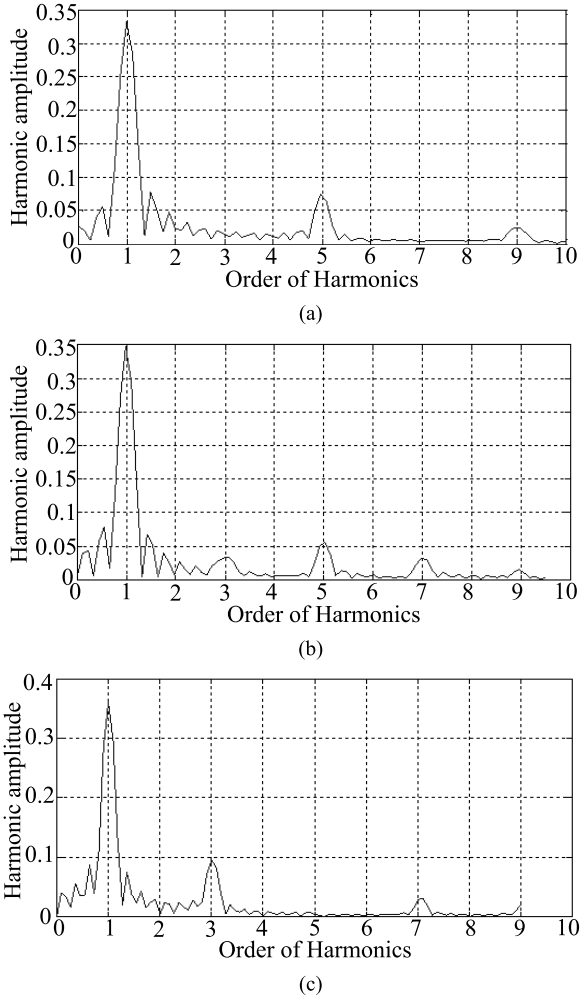

Fig. 6. Corresponding FFT results of the air gap flux density. (a) FFT result of the air gap flux density for the single-layer Halbach PM array ($n = 1$). (b) and (c) FFT results of the air gap flux density for the double-layer PM arrays with different n. (a) $n = 1$. (b) $n = 0.7$. (c) $n = 0.4$.

the performance of the linear motor. To further study the distribution characteristics of the AGMFD, the waveform of the air gap flux density is analyzed by the FE model. The simulated results of three structures are shown in Fig. 5.

It can be seen that the air gap magnetic field has a relatively obvious saddle-shaped distribution and distortion of the end for the single-layer array and the double-layer arrays with $n = 0.7$. The end effect is a major factor for causing the fluctuation of the electromagnetic force. In addition, the simulated results show that the peak of the magnetic field waveform for the double-layer PM arrays is slightly higher than that of the single-layer array. The fast Fourier transform (FFT) is performed on the waveform of the magnetic field in Fig. 5, and the corresponding FFT results are shown in Fig. 6.

As can be seen from Fig. 6, the waveform of the magnetic field for a single-layer PM array includes high-order harmonics such as the fundamental wave, the fifth harmonic, and the ninth harmonic, which are consistent with the results of the analytical calculation. The amplitude of the fundamental wave for the double-layer PM arrays is higher than that of the single-layer PM array, but the distribution of the higher-order harmonic for different double-layer arrays is different.

TABLE I

FUNDAMENTAL WAVE AND HARMONIC DISTRIBUTION OF AGMFD

n	Fundamental amplitude (T)	Major harmonic order	Harmonic amplitude (T)	Harmonic/ Fundamental
0.2	0.303	3	0.098	32.3%
0.3	0.328	3	0.092	28%
0.4	0.359	3	0.096	26.7%
0.5	0.339	3	0.069	20.35%
0.6	0.355	3、5	0.069	19.4%
0.7	0.344	5	0.063	18.3%
0.8	0.333	5	0.06	18%
0.9	0.349	5	0.065	18.6%
1	0.332	5	0.067	20.2%

The waveform of the magnetic field for the double-layer PM arrays with $n = 0.7$ mainly includes the fifth and seventh harmonics, while that of the double-layer PM arrays with $n = 0.4$ mainly includes the third and seventh harmonics.

Similarly, the waveforms of the magnetic field for other PM arrays are sampled and analyzed by FEM. The amplitude of the fundamental wave and main high harmonics for nine types of PM arrays are obtained as shown in Table I. The results show that the amplitude of the fundamental wave increases first and then decreases with the increase of n;

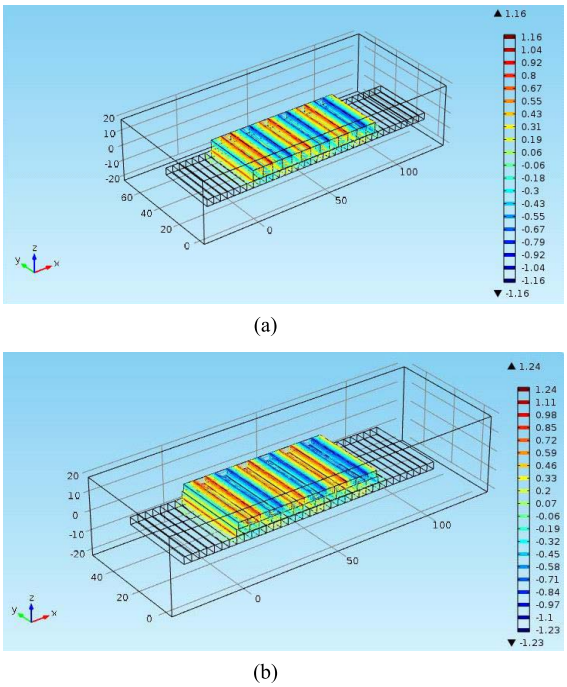

Fig. 7. 3-D FEM of two linear motors. (a) A single-layer Halbach array. (b) An optimized two-layer Halbach array.

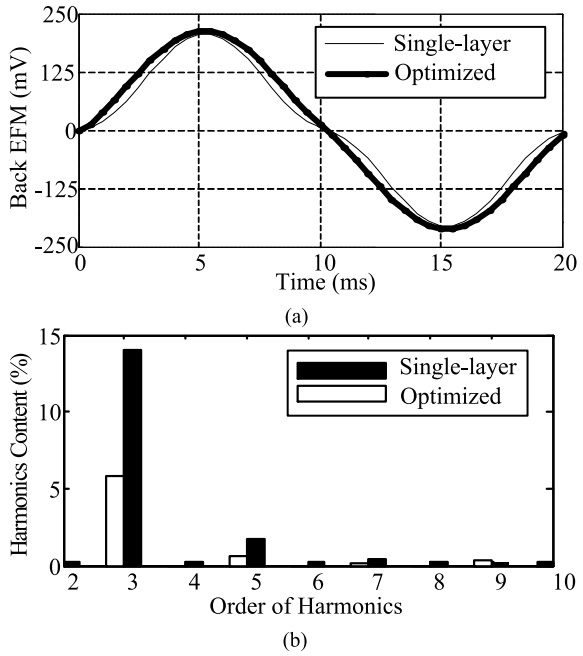

Fig. 8. Back EMF and the corresponding harmonic content of two linear motors. (a) Voltage waveform of the initial and optimized and (b) the corresponding harmonic content.

however, the ratio of the harmonic amplitude and the fundamental amplitude decreases first and then increases. The smaller the ratio, the better sinusoidal characteristics the waveform of the magnetic field has. At the same time, the smaller the value of n, the smaller the volume of the magnet, and the lighter the weight is. Therefore, the width ratio of the PM can be practically $n = 0.7$, that is, the width of the small-sized PM is 4.62 mm. However, the width of the small-sized PM can be set to 4.6 mm by considering the difficulty in processing.

V. Analysis of Performance

The 3-D model of two linear motors with a traditional single-layer Halbach PM array and with optimized double-layer Halbach PM arrays is established in FE software. The single-layer Halbach PM array is composed of 13 PMs, and the double-layer Halbach PM arrays are composed of 26 PMs that are stacked up and down. Three-phase currents were applied to the armature windings, and the magnetic field of the two motors was simulated and analyzed, as shown in Fig. 7.

A. Back Electromotive Force

Fig. 8(a) shows the back EMF waveform of the initial structure and that of the optimized structure, with the corresponding harmonic content shown in Fig. 8(b). The initial structure is the linear motor with common single-layer Halbach PM arrays. The results show that the total harmonic distortion of the optimized waveform for the EMF has been decreased significantly from 14.43% to 4.95%.

B. Electromagnetic Thrust

The electromagnetic thrust of the PMLM with a single-layer Halbach PM array and that of the PMLM with the optimized double-layer Halbach PM arrays are shown in Fig. 9. The results show that the thrust fluctuation of the PMLM with the optimized double-layer Halbach PM arrays is obviously less than that of the PMLM with a single-layer Halbach PM array, and the amplitude of the electromagnetic thrust for the PMLM with the optimized double-layer Halbach PM arrays is a little more than that of the electromagnetic thrust for the PMLM with a single-layer Halbach PM array.

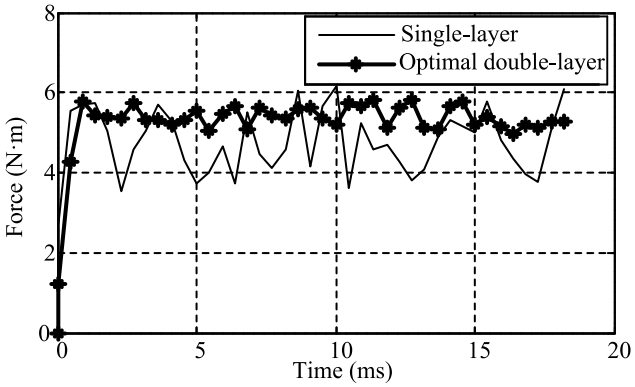

Fig. 9. Electromagnetic thrust of two linear motors.

The simulations reveal that the performances of the PMLM have been improved when the optimized double-layer Halbach PM array is used for the PMLM.

VI. Experiment

The experiment is carried out in order to verify the simulated results. The prototype of the PMLM with a single-layer Halbach PM array and that of the PMLM with the optimized double-layer Halbach PM arrays are made. Fig. 10 shows

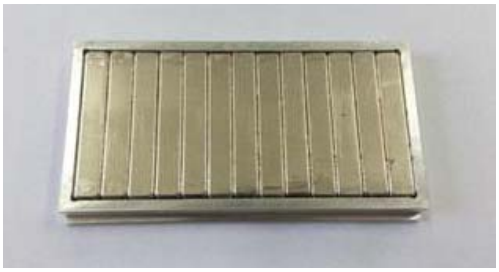

(a)

(b)

Fig. 10. Prototypes of single-layer and double-layer Halbach PM arrays. (a) Single-layer Halbach array. (b) Optimized two-layer Halbach array.

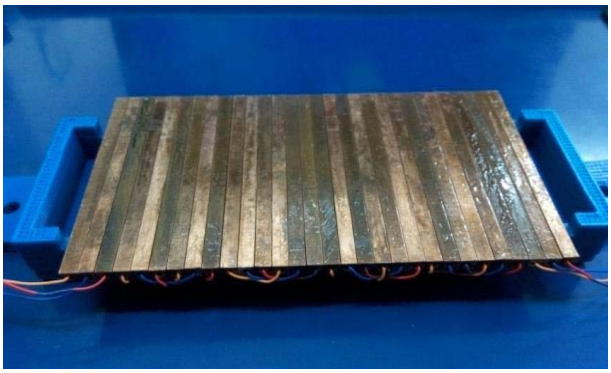

Fig. 11. Physical diagram of the stator of the motor.

prototypes of single-layer and optimized double-layer Halbach PM arrays.

When the double-layer Halbach PM arrays are fabricated, the magnetizing direction of the PM cannot be mistaken, otherwise the performance of the motor will be affected. In addition, when the PM is assembled with too much force, the PM will be destroyed. It can be seen that the surface flatness of the PM array is good, the magnetic block is evenly arranged, and the sizes of single-layer and double-layer Halbach PM arrays are processed according to the initial size and the optimal size of Halbach PM arrays. Fig. 11 is a physical diagram of the stator. The PMLM with a single-layer Halbach PM array and the PMLM with the optimized double-layer Halbach PM array have the same stator.

The back EMF was carried out on the two prototypes, the experimental system is shown in Fig. 12. The measured results of back EMF are shown in Fig. 13, where the green waveform represents the back EMF waveform of the linear motor with a common single-layer Halbach PM array and the yellow waveform represents the back EMF waveform of the linear motor with optimized double-layer Halbach PM arrays.

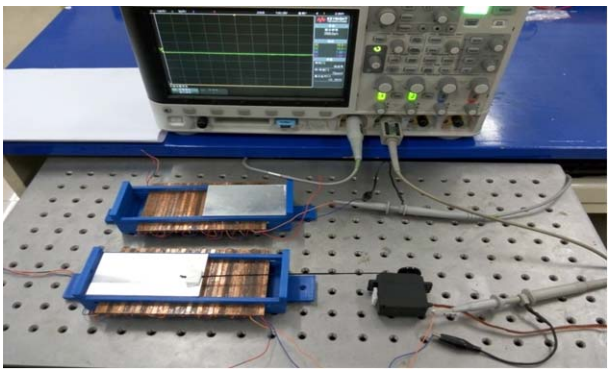

Fig. 12. Experiment platform.

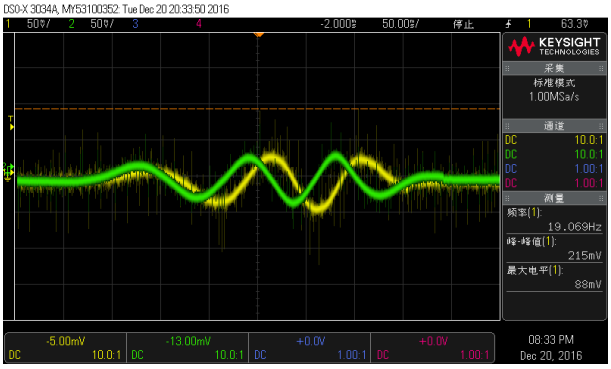

Fig. 13. Measurement results of back EMF.

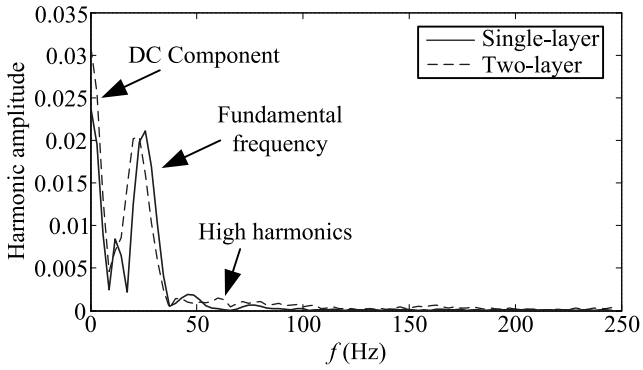

Fig. 14. Harmonic distribution of the back EMF waveform.

It can be seen that the peak values of the two back EMF waveforms are substantially equal, and the peak-to-peak value is at most 215 mv. The two waveforms have similar regularity and good sinusoidal characteristics, which verify the correctness and the feasibility of the prototype processing.

It is difficult to intuitively distinguish the advantages and disadvantages of the two waveforms, so they are analyzed by FFT. The harmonic characteristics of the waveform are obtained, as shown in Fig. 14.

As seen in Fig. 14, both the direct current (dc) component and the high harmonics of the back EMF for the linear motor with optimized double-layer Halbach PM arrays are lower than those of the back EMF for the linear motor with a common single-layer Halbach PM array. However, the dc component in alternating current (ac) can destroy the balance of the

magnetic field, so that the motor is prone to vibration. The high harmonics of the back EMF can reduce the efficiency and increase the additional loss of motor. Therefore, the lower the dc component and high harmonics of the back EMF, the better the performance of the motor. In addition, the fundamental frequency of the back EMF for the linear motor with optimized double-layer Halbach PM arrays is higher than that of the back EMF for the linear motor with a common single-layer Halbach PM array. So, the linear motor with optimized double-layer Halbach PM arrays can obtain better sinusoidal waves and a higher amplitude for the back EMF than the linear motor with a common single-layer Halbach PM array, which is consistent with the FE simulated results.

Regarding cost, the two motors have the same stator, but a different mover. The single-layer Halbach PM array is composed of 13 PMs that are 40 mm long, 6.6 mm wide, and 6.6 mm high, so the total volume of 13 PMs used in the single-layer Halbach PM array is 22 651.2 mm^3. However, the optimized double-layer Halbach PM arrays are composed of 26 PMs; 13 PMs that are 40 mm long, 6.6 mm wide, and 3.3 mm high, and the other 13 PMs that are 40 mm long, 4.6 mm wide, and 3.3 mm high. The total volume of 26 PMs used in the optimized double-layer Halbach PM arrays is 19 219.2 mm^3. The results show that the usage of PMs of the optimized double-layer Halbach PM arrays is significantly less than that of the single-layer Halbach PM array. Therefore, the cost of the PMLM with optimized double-layer Halbach PM arrays is less than that of the PMLM with the single-layer Halbach PM array.

VII. Conclusion

In this paper, a linear motor with optimized two-layer Halbach PM arrays is proposed for direct-drive applications. The air gap magnetic field of the linear motor with various structures of PM arrays is simulated and compared by the FEM, thus the optimized structure of Halbach PM arrays is confirmed. The 3-D FEMs of PMLMs with traditional single-layer Halbach PM arrays and the optimized double-layer Halbach PM arrays are established, respectively. The EMF and the electromagnetic thrust of the PMLM have been improved when the optimized double-layer Halbach PM array is used for the PMLM. Finally, the experimental results are found to be consistent with the FE simulated results, and the cost of the two PMLMs is analyzed. It is verified that the PMLM with optimized double-layer Halbach PM arrays not only shows better performances but also have lower cost than the PMLM with a single-layer Halbach PM array. With the high-end machining technology, the PMLM with optimized double-layer Halbach PM arrays is well suitable for direct-drive systems.

Acknowledgment

This work was supported in part by the National Natural Science Foundation of China under Grant 51807124, in part by the Natural Science Foundation of China's Hebei Province under Grant E2018210162, in part by the Young Foundation of Education Department of China's Hebei Province under Grant QN2018226, and in part by the Postgraduates Innovation Fund of Shijiazhuang Tiedao University.

References

[1] Q. Wang, Y. Xu, Y. Li, and J. Zou, "Design criteria, modeling, and verification of tubular transverse flux machines for force-to-current ratio improvement in direct drive applications," *IEEE Trans. Magn.*, vol. 52, no. 7, Jul. 2016, Art. no. 8203004.

[2] Y. Gao, R. Qu, D. Li, and F. Chen, "Force ripple minimization of a linear Vernier permanent magnet machine for direct-drive servo applications," *IEEE Trans. Magn.*, vol. 53, no. 6, Jun. 2017, Art. no. 7001905.

[3] G. De Donato *et al.*, "Ω-shaped axial-flux permanent-magnet machine for direct-drive applications with constrained shaft height," *IEEE Trans. Ind. Appl.*, vol. 51, no. 4, pp. 3050–3058, Jul./Aug. 2015.

[4] R. Cao, Y. Jin, M. Lu, and Z. Zhang, "Quantitative comparison of linear flux-switching permanent magnet motor with linear induction motor for electromagnetic launch system," *IEEE Trans. Ind. Electron.*, vol. 65, no. 9, pp. 7569–7578, Sep. 2018.

[5] L. Xu, G. Liu, W. Zhao, J. Ji, and Z. Ling, "Analysis of new modular linear flux reversal permanent magnet motors," *IEEE Trans. Magn.*, vol. 51, no. 11, Nov. 2015, Art. no. 8109904.

[6] I.-U.-R. Usman and X. Lu, "Force ripple attenuation of 6-DOF direct drive permanent magnet planar levitating synchronous motors," *IEEE Trans. Magn.*, vol. 51, no. 12, Dec. 2015, Art. no. 8208708.

[7] Q. Wang, B. Zhao, H. Zhao, Y. Li, and J. Zou, "Optimal design of tubular transverse flux motors with low cogging forces for direct drive applications," *IEEE Trans. Appl. Supercond.*, vol. 26, no. 7, 2016, Art. no. 0609005.

[8] Q. Liu *et al.*, "Cogging force reduction of double-sided linear flux-switching permanent magnet machine for direct drives," *IEEE Trans. Magn.*, vol. 49, no. 5, pp. 2275–2278, May 2013.

[9] C. S. Cyusa and Y. Fujimoto, "Enactment-based direct-drive test of a novel radial-gap helical rotlin machine," *IEEE Trans. Ind. Appl.*, vol. 54, no. 2, pp. 1273–1282, Mar./Apr. 2018.

[10] M. A. M. Cheema, J. E. Fletcher, D. Xiao, and M. F. Rahman, "A linear quadratic regulator-based optimal direct thrust force control of linear permanent-magnet synchronous motor," *IEEE Trans. Ind. Electron.*, vol. 63, no. 5, pp. 2722–2733, May 2016.

[11] Y. Xu, H. Yan, and J. Zou, "A fault tolerant control strategy for six-phase transverse flux tubular PMLM based on synthetic vector method," *IEEE Trans. Plasma Sci.*, vol. 43, no. 5, pp. 1332–1338, May 2015.

[12] Y. Yao and Q. Lu, "Comparative study of E-core and C-core modular PM linear machines with different slot/pole combinations," *IEEE Trans. Magn.*, vol. 53, no. 11, Nov. 2017, Art. no. 8110307.

[13] L. Zeng, X. Chen, X. Li, W. Jiang, and X. Luo, "A thrust force analysis method for permanent magnet linear motor using schwarz–christoffel mapping and considering slotting effect, end effect, and magnet shape," *IEEE Trans. Magn.*, vol. 51, no. 9, Sep. 2015, Art. no. 8107609.

[14] H. Du, X. Chen, G. Wen, X. Yu, and J. Lü, "Discrete-time fast terminal sliding mode control for permanent magnet linear motor," *IEEE Trans. Ind. Electron.*, vol. 65, no. 12, pp. 9916–9927, Dec. 2018.

[15] C. Wen *et al.*, "Coil shape optimization for superconducting wind turbine generator using response surface methodology and particle swarm optimization," *IEEE Trans. Appl. Supercond.*, vol. 24, no. 3, Jun. 2014, Art. no. 5202404.